Applied Surface Science 256 (2010) 6459–6465

Contents lists available at ScienceDirect

Applied Surface Science

journal homepage: www.elsevier.com/locate/apsusc

Study of the adsorption, electronic structure and bonding of C_2H_4 on the FeNi(1 1 1) surface

S. Simonetti[a,b,*], G. Brizuela[b,1], A. Juan[b,1]

[a] Universidad Tecnológica Nacional, 11 de Abril 461, 8000 Bahía Blanca, Argentina
[b] Universidad Nacional del Sur, Av. Alem 1253, 8000 Bahía Blanca, Argentina

ARTICLE INFO

Article history:
Received 25 February 2010
Received in revised form 27 March 2010
Accepted 9 April 2010
Available online 21 April 2010

Keywords:
Alloy
Iron
Nickel
Carburization
Modelling studies

ABSTRACT

The adsorption of C_2H_4 on the FeNi(1 1 1) alloy surface has been studied by ASED-MO tight binding calculations. The C_2H_4 molecule presents its most stable geometry with the C=C bond axis parallel to the surface along the [1, −1, 0] direction, bonded on top Fe atom and bonded along a Fe–Fe bridge site. As a consequence, the strength of the local Fe–Fe bond decreases between 37 and 62% of its original bulk value. This bond weakening is mainly due to the new C–Fe interactions however no Fe_3C carbide formation is evidenced on surface. The Fe–Ni and Ni–Ni superficial bonds are only slightly modified.

1. Introduction

The used materials for industrial process that involve carburization are generally Fe- and Ni-based alloys that offer high corrosion and creep resistance. When the material is exposed to gases containing carbon, e.g. CH_4, C_2H_4, it can pick up carbon. The degree of carburization is governed by the levels of carbon in the gas, the temperature and the steel composition. The carbon which is picked up by the steel will largely form carbides. The resistance to thermal cycling is reduced and there is a danger of cracks developing in the material.

A study was carried out to investigate the carbon deposition on nickel-, cobalt-, molybdenum-, and iron-based alloy foils during thermal stressing. Temperature-programmed oxidation analysis and scanning electron microscopy examination showed that the amount of carbon deposited on metal foils decreased in the order Inconel 600 > Havar > Fecralloy > Waspaloy > Hastelloy-C > MoRe > Inconel 718 [1]. Besides, lower carburization resistance below 1000 °C was manifested by increased carbon pick-up and degradation of mechanical properties of alloy Haynes-214 [2].

Metal dusting corrosion of nickel-based alloys has been simulated in high-carbon-activity environments over a temperature range of 450–750 °C. Overall, Ni-based alloys corrode by a combination of carbon diffusion and precipitation in the alloy interior and atom migration through surface carbon deposits. The mechanistic aspects of metal dusting are discussed with particular attention to the stages of microstructure evolution as degradation proceeds [3].

The behaviour of carbon deposition on preoxidized Fe–Ni alloys exposed to CH_4–H_2 mixture at 1203 K was studied by metallography and thermogravimetry [4]. It was reported that nickel retards the carburization and carbon deposition by lowering the solubility limit of graphite in austenite and by reducing catalytic activity for the pyrolytic reaction of CH_4. The decomposition of a $C_2H_4/CO/H_2$ reactant mixture over a series of Fe–Ni catalysts has been studied and the analysis reveals that the addition of CO to a C_2H_4/H_2 feed results in a substantial increase in the decomposition of the olefin over all the bimetallic powders being this effect most pronounced on the iron-rich systems [5]. The major product from this series of Fe–Ni catalysts was found to be solid carbon in the form of various filamentous structures.

The adsorption and decomposition of ethylene on Fe(1 0 0) was studied by a combined UV photoemission and molecular orbital analysis [6–8]. The adsorption of C_2H_4 on the clean, C- and O-covered Fe(1 0 0) surface was studied using HREELS, with additional information provided by TPD, AES and LEED. On the clean surface, C_2H_4 adsorbed molecularly on this surface in a di-sigma-bonded C_2H_4 desorbed at 240 K or decomposed to form the methylidyne (CH) and ethynyl (CCH) species below 260 K. Preadsorbed carbon

* Corresponding author at: Departamento de Física, Universidad Nacional del Sur, Av. Alem 1253, 8000 Bahía Blanca, Argentina. Tel.: +54 291 4595141; fax: +54 291 4595142.
E-mail address: ssimonet@uns.edu.ar (S. Simonetti).
[1] Tel.: +54 291 4595141; fax: +54 291 4595142.

0169-4332/$ – see front matter © 2010 Elsevier B.V. All rights reserved.
doi:10.1016/j.apsusc.2010.04.035

and oxygen block the chemisorption of di-sigma-bonded C_2H_4 and induce physisorption of C_2H_4 at 100 K [9]. Adsorption of ethylene on Fe(1 1 0) [10] and Fe(1 1 1) [11] has been previously studied using HREELS. The adsorption and reactions of organic fragments containing C_2 unit on the iron surface have been investigated employing periodic density functional theory. The calculations proved that the most favourable C_2 species on the Fe(1 0 0) surface are those containing the acetylenic carbon at the position: C–CH, $C–CH_2$, and $C–CH_3$. This computational study indicates that the production of ethane is preferred over ethylene, which agrees with the product selectivity observed in the industrial Fischer–Tropsch synthesis catalyzed by iron [12].

The adsorption sites of ethylene on the Ni(1 1 0) surface were determined by theoretical cluster calculations. At low coverage, an isolated ethylene molecule occupies a site approximately midway between short-bridge and atop sites; while at high coverage (0.5 ML), the local adsorption sites are found to be similar to that at low coverage but the C–C bond lengths are different. The C–C-axis of molecule is slightly parallel to the ridges and offset in ⟨1 0 0⟩ direction [13]. Low-energy electron diffraction (LEED), angle-resolved ultraviolet photoemission spectroscopy (ARUPS), and near-edge X-ray-absorption fine structure (NEXAFS) investigation revels that the ethylene molecules on Ni(110) are adsorbed with the molecular plane parallel to the surface and the C–C axis preferentially aligned along the [1–10] direction of the substrate [14].

The multiple-scattering cluster method was used to study ethylene adsorbed on the Ni(1 0 0) surface. The result showed that the molecule is adsorbed on the perpendicular bridge site, and the distance between the C atom and the nearest Ni atom is 1.70 Å, while the molecular plane tilting to the surface is 50°. It was also reported that the interaction between hydrogen atom and Ni substrate plays an important role in the formation of the adsorption structure [15]. Temperature-programmed X-ray photoelectron spectroscopy was used to study the thermal chemistry of ethylene on Ni(1 0 0) in the temperature range 90–530 K. For the dehydrogenation of ethylene, a vinyl species (C_2H_3) is observed. Carbidic carbon is formed as the final dehydrogenation product [16].

First principles density functional theory calculations was performed for the chemisorption of ethylene on the {1 1 1}, {1 0 0} and {1 1 0} surfaces of Pd [17]. On all the three low-index surfaces, the most stable site and geometry for C_2H_4 is that where the C–C bond axis is parallel to the surface along the bridge site. In addition, the adsorption of ethylene on Au–Pd alloys formed on a Pd(1 1 1) surface was investigated using a combination of temperature-programmed desorption (TPD) and reflection absorption infrared spectroscopy (RAIRS) [18]. For gold coverages greater than 0.7, ethylene adsorbs primarily on gold sites. At gold coverages between 0.5 and 0.7, ethylene is detected on palladium sites in a π-bonded configuration.

Carburization is the most common cause of failure of cracking tubes for ethylene (C_2H_4) production and can drastically reduce the life of metal components. Metal dusting results from oversaturation of metals and alloys with C activities >1 leads to disintegration of the materials in a dust of metal particles, graphite, and sometimes oxides and carbides. The latter are formed in a preceding carburization from the alloying elements forming stable carbides. The remaining Fe–Ni matrix is destroyed by the graphite formation, either via cementite (Fe_3C) as intermediate or in the case of Ni-based alloys by direct inward growth of graphite. During carburization and metal dusting, the dissolution and diffusion of C into the metal phase are important steps [19].

A combination of flow reactor studies and electron microscopy techniques were used to investigate the way the composition of iron-nickel alloy particles influence the growth characteristics of carbon deposits formed during the decomposition of ethane at temperatures over the range 815–865 °C. Major differences in the selectivity patterns of alloys were evident with the amount of catalytically produced solid carbon being significantly higher on a Fe–Ni (5:5) powder than on a Fe–Ni (8:2) sample. Examination of the deposit revealed the existence of two types of structures, carbon nanofibers and a graphite shell-like material, both of which contained associated metal particles [20].

Ab initio calculations determine the equilibrium geometries, binding energies and the phase stability in the Fe–Ni system [21,22]. In a previous works, our group has performed a preliminary computational study of the C location on the FeNi(1 1 1) surface and in the vicinity of an FeNi bulk vacancy. The addition of a C atom in the FeNi matrix containing a vacancy decreases the strength of the Fe–Fe bond locally to about 80% of its original bulk value. This bond weakening is mainly a consequence of the C–Fe interaction. On the other hand, the energy minimum location of the C atom on the FeNi(1 1 1) was found at 1.60 Å from the surface. The main interaction is again the C–Fe and the C-surface bonding achieved at the expense of the weakening of the Fe–Ni nearest neighbours bond to C, which decreases to about 52% of its bulk value [23].

In this paper we studied by ASED-MO tight binding calculations, the C_2H_4 chemisorption on the FeNi(1 1 1) alloy surface. We also analyzed the electronic structure and bonding during the adsorption phenomena. The theory and model are described in the next section.

2. Theoretical method and adsorption model

The ambient-pressure temperature composition structural phase diagram of FeNi is complicated and is still being elaborated [24,25]. It includes a Fe-rich body-centred cubic (BCC) phase (α-phase), a face-centred-cubic (FCC) phase (γ-phase) that can be metastably quenched over a broad composition range 0–70 at% Fe at room temperature; INVAR and ELENVAR are two such alloys; a low spin FCC phase (γLS-phase) and chemically ordered FCC phases centred at ∼50 and ∼25 at% Fe (FeNi and $FeNi_3$ phases, respectively). Also, a chemically ordered Fe_3Ni FCC phase has been proposed but its existence has never been substantiated by experimental evidence. In addition, high pressures stabilize a non-magnetic hexagonal close packed (HCP) phase (ε-phase) [25–28] that is closely related to the γ-LS-phase [25]. Vaderruten et al. [29] determined the coexistence of BCC and FCC phases in the range of $22 < x < 40$ at% Ni. The reported experimental lattice parameter in BCC phase is 2.86 Å, while for the FCC is 3.59 Å. These parameters are concentration independent due to the similarity in the Fe and Ni atomic size in such a way that Fe or Ni interchange does not affect the lattice parameters. The changes in the magnetic properties follow the changes in chemical composition and BCC or FCC phases. The same authors found that the BCC phase is ferromagnetic, while the FCC is ferro or paramagnetic. Dang and Rancourt performed ab initio calculation in the FeNi phase (CuAu(I)) reporting a lattice parameter $a = 3.592$ Å [30]. We notice that the FeNi structure no longer has cubic symmetry but is, in fact, tetragonal (L10). In this work, it was considered as having cubic structure because the distortion is small [29,30] (see Fig. 1(a)).

Our calculations were performed using the ASED-MO method an approximate molecular orbital tight binding scheme [31]. This method captures well the essential orbital interactions in chemisorption. The interaction between the C_2H_4 molecule and the FeNi(1 1 1) surface was studied using a two dimensional slab of finite thickness, so as to better simulate the semi-infinite nature of the metallic surface. A three-layer slab was employed as a compromise between computational economy and reasonable accuracy. The FeNi(1 1 1) surface was represented by a 108 atoms (50:50) distributed in three layers (FCC arrangement) of 36 atoms. The computed lattice parameter for the FCC phase is very close to recent

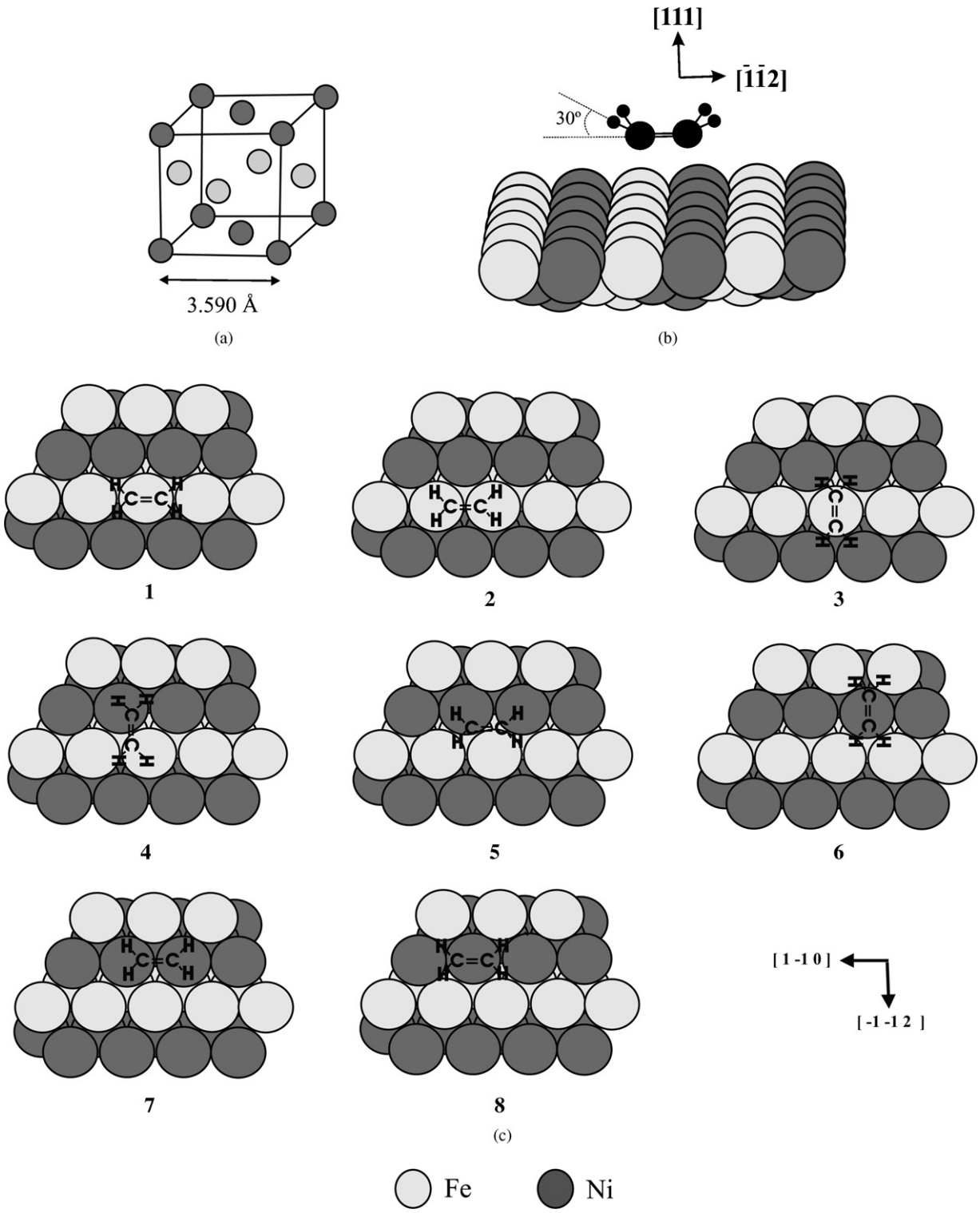

Fig. 1. Schematic (a) unit cell, (b) lateral view and (c) top view of the C_2H_4 adsorption configurations on the FeNi(1 1 1) surface.

XRD and Mossbauer measurements (a = 3.590 Å vs. 3. 605 Å [32]). The distance between planes was 2.074 Å. After adsorption, the surface reconstructs with an outward displacement for the first layer of 0.12 and 0.10 Å for the second layer. The geometry for ethylene in the vacuum was taken from the literature data: C–C = 1.34 Å, C–H = 1.09 Å, and H–C–H = 117.8° [33]. The free C_2H_4 molecule that is flat in the vacuum, during adsorption presents a C=C–H tilt angle of 30° with respect to the FeNi(1 1 1) plane (see Fig. 1(b)) in such a way that the molecule has its double C=C bond near to the metal surface. Eight adsorption configurations were selected for the present study (see Fig. 1(c)) and the molecule was adsorbed on one side of the slab.

The adsorption energy E_{ads} values were calculated from the energy difference:

$$\Delta E_{ads} = E_T(C_2H_4/FeNi) - E_T(FeNi) - E_T(C_2H_4) \quad (1)$$

Table 1
Equilibrium chemisorptive properties for C_2H_4 on FeNi(1 1 1).

	Configurations							
	1	2	3	4	5	6	7	8
E_{abs} (eV)	−8.82	−8.63	−7.73	−5.80	−5.31	−5.08	−4.33	−4.33
$d_{C\text{-surface}}$ (Å)	1.60	1.70	1.60	1.70	1.60	1.70	1.80	1.70

where C_2H_4/FeNi, C_2H_4 and FeNi refer to molecule-on-slab system, the free molecule and the bare iron-nickel surface, respectively.

The density of states (DOS) and the crystal orbital overlap population (COOP) curves for the C_2H_4/FeNi system were calculated in order to analyze the adsorbate-surface interactions using the YAeHMOP code [34]. The COOP curve is an energy-resolved plot of the overlap population-weighted density of states. Integration of the COOP curve up to the Fermi level gives the total overlap population (OP).

3. Results and discussions

The optimum adsorption geometries for the C_2H_4 molecule on the FeNi(1 1 1) surface is shown in Fig. 1(c). Table 1 presents the adsorption minimum energy and the corresponding C_2H_4–FeNi(1 1 1) distance for each configuration. We can see that configurations 1 and 2 are the most stables. The energies difference is 0.19 eV while the equilibrium distances from C=C to the surface are 1.60 and 1.70 Å, respectively. The most stable sites and geometries for C_2H_4 contain the C=C bond axis parallel to the surface along the [1, −1, 0] direction, are on Fe top site (configuration 1) and along the Fe–Fe bridge site (configuration 2). A general picture in favour of molecularly π-bonded and di-σ bonded ethylene, respectively, is obtained from these results.

Regarding the electronic structure, we calculated the density of states (DOS) and the crystal orbital overlap population (COOP) curves for the C_2H_4/FeNi system in order to analyze the adsorbate-surface interactions. Fig. 2 shows the DOS plots for the C_2H_4/FeNi(1 1 1) system. The alloy d states form a band starting at −14 eV with a bandwidth of 7 eV. If we compare both, the total DOS shown in Fig. 2(a) and (b), the more noticeable differences are the three small peaks that appear at about −15, −17 and −19 eV respectively, that corresponds to the C and H states from the C_2H_4 molecule after adsorption. The small contribution of the C_2H_4 to DOS is due to its low concentration. Fig. 2(c) presents a plot of these projections. The Fermi energy of the metal surface moves slightly, because of the finite thickness of the slab and electron transfer between slab and adsorbate.

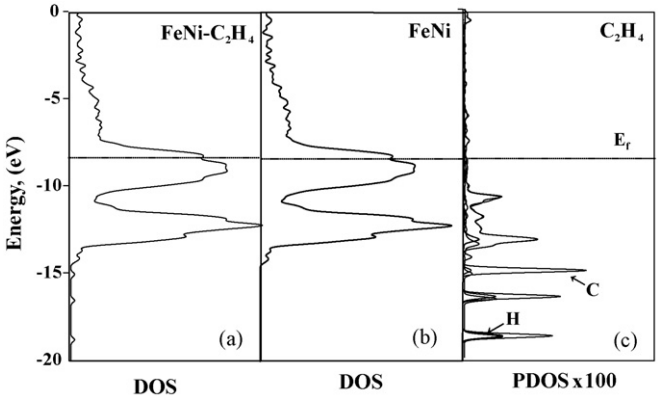

Fig. 2. (a) Total DOS for the FeNi/C_2H_4 system, (b) total DOS for the clean FeNi surface and (c) projected DOS for C_2H_4 on the FeNi surface.

Tables 2 and 3 present the atomic orbital occupation and the OP values for the atoms that participate in the C_2H_4/FeNi adsorption. For configuration 1, both C atoms bond on atop Fe_{II} with OP of 0.187 and 0.182, respectively. C_{II} and C_I also bind with Fe_I and Fe_{IInn} respectively, having both C–Fe OP values of 0.123. The COOP curves for these C–Fe interactions are shown in Fig. 3(a)–(d). The C–Fe_{II} interactions mainly involve p_x and p_z orbitals of Fe_{II} whose populations decrease 98% comparing with the clean surface. The s and d_{xz} populations of Fe_{II} decrease to about 37%, the d_{yz}, p_y and d_{z^2} populations decrease to about 21–25%, while $d_{x^2-y^2}$ and d_{xy} populations are modified 15–18%. The Fe_I and Fe_{IInn} orbital occupations are modified in a lesser extent because the C atoms do not locate on atop of these atoms; the major changes are noticed in p_x, p_y and d_{yz} atomic orbitals of Fe_I and Fe_{IInn}. We can conclude that the major changes are due to C–Fe_{II} interactions that are mainly formed at expense of the Fe–Fe neighbouring bonds whose strength decreases between 37 and 43% (see Table 3). The Fe–Ni nearest neighbouring bond strength decreases only a 9%. No evidence of C–Ni interactions is detected in the FeNi(1 1 1) surface. The presence of nickel in the alloy composition reduces the C accumulation. Nickel prevents carburization and carbon deposi-

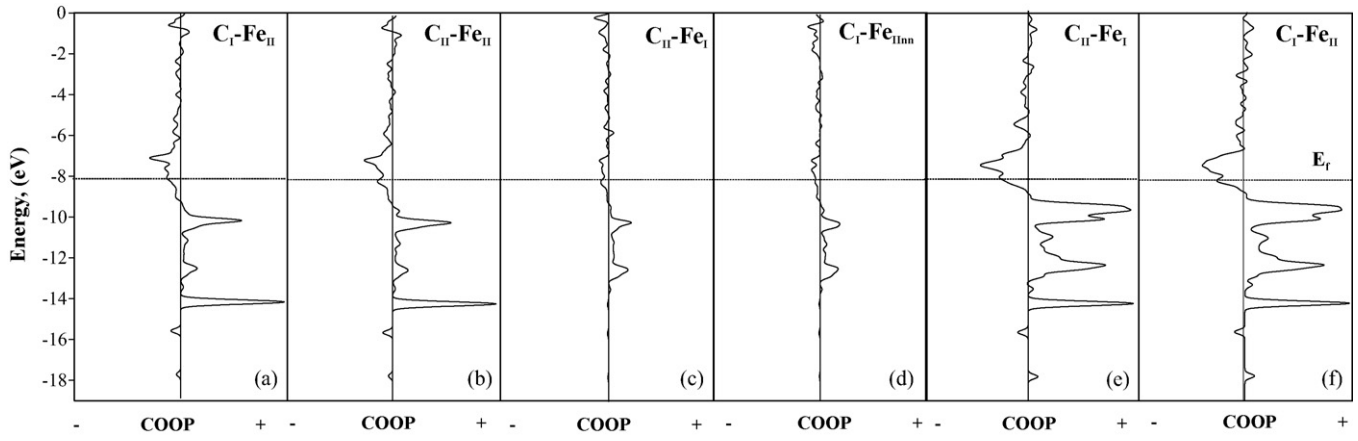

Fig. 3. (a)–(d) COOP curves for C–Fe interactions for configuration 1. (e) and (f) COOP curves for C–Fe interactions for configuration 2.

Table 2
Atomic orbital occupations for the C_2H_4/FeNi chemisorption system.

	s	p_x	p_y	p_z	$d_{x^2-y^2}$	d_{z^2}	d_{xy}	d_{xz}	d_{yz}
Fe_I	0.532	0.058	0.007	0.035	1.107	1.107	0.979	1.235	0.929[a]
	0.491	0.023	0.001	0.005	1.098	1.048	0.994	0.833	0.865[b]
	0.594	0.081	0.033	0.042	1.134	1.133	0.994	1.313	1.157[c]
Fe_{II}	0.375	0.001	0.024	0.001	1.001	0.816	0.814	0.805	0.911[a]
	0.491	0.023	0.001	0.005	1.121	1.053	0.979	0.878	0.849[b]
	0.594	0.080	0.031	0.040	1.173	1.091	0.990	1.286	1.155[c]
Ni_I	0.846	0.313	0.311	0.298	1.886	1.860	1.863	1.906	1.905[a]
	0.849	0.314	0.306	0.300	1.887	1.862	1.861	1.908	1.901[b]
	0.833	0.312	0.307	0.301	1.891	1.863	1.863	1.917	1.910[c]
Ni_{Inn}	0.871	0.314	0.364	0.239	1.892	1.916	1.872	1.945	1.933[a]
	0.867	0.296	0.351	0.212	1.895	1.920	1.872	1.943	1.935[b]
	0.921	0.352	0.375	0.293	1.886	1.924	1.869	1.942	1.932[c]
C_I	1.021	1.113	1.058	1.212[a]					
	1.016	1.119	1.106	1.270[b]					
	0.956	1.170	1.143	0.928[d]					
C_{II}	1.021	1.114	1.057	1.208[a]					
	1.016	1.120	1.106	1.269[b]					
	0.956	1.170	1.143	0.928[d]					
H_I	0.949[a]								
	0.944[b]								
	0.901[d]								
H_{II}	0.950[a]								
	0.944[b]								
	0.901[d]								
H_{III}	0.950[a]								
	0.946[b]								
	0.901[d]								
H_{IV}	0.950[a]								
	0.944[b]								
	[d]								

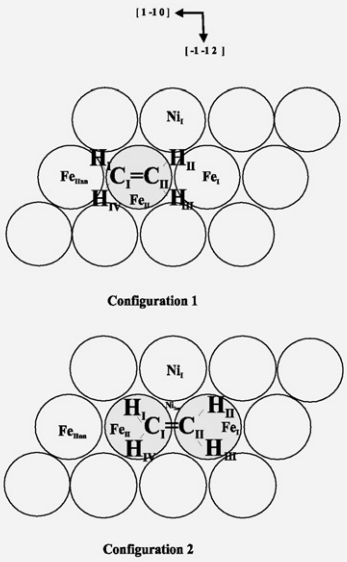

[a] C_2H_4 adsorbed on FeNi according to configuration 1.
[b] C_2H_4 adsorbed on FeNi according to configuration 2.
[c] FeNi isolated surface.
[d] C_2H_4 in the vacuum.

tion by reducing catalytic activity for the reaction of C_2H_4 on the surface. A study reveals that Ni and Fe may act as either competing or cooperative catalyst components in the process of carbon nanotubes growth on Ni–Fe based steel alloy. During partial oxidation of methane it is resulted in suppression of Ni catalytic activity in favour of Fe. Interaction between Ni and Fe during non-oxidative conversion leads to cooperative effect; the activity of bimetallic catalyst increases as compared with monometallic one [35].

There is an electron transfer from Fe and Ni nearest neighbours to the C atoms. On the other hand, the H-surface interactions are almost negligible (they have a very small OP values) which is due to the long H-surface distance. Furthermore, the tilted geometrical configuration adopted for the molecule during adsorption prevents any H-surface interactions.

For configuration 2, the C atoms locate on Fe_I–Fe_{II} bridge site, both C_I–Fe_{II} and C_{II}–Fe_I OPs are similar (about 0.44) and, higher than in configuration 1 (see Fig. 3(e) and (f)). After adsorption, the most affected is the p_y orbital of Fe_I and Fe_{II} whose populations decrease a 97%. The p_x and p_z orbital populations of Fe_I and Fe_{II}, decrease between 70 and 88%; while the d_{yz} and d_{xz} populations decrease to about 25–37%. The s population decreases 17%. The Fe_I–Fe_{II} OP decrease to about 62% due the C_I–Fe_{II} and C_{II}–Fe_I interactions formed on the FeNi(1 1 1) surface. The others Fe–Fe nearest neighbour bonded to the C atoms, only decrease their OP to 3%. The Fe_I–Ni_I and Fe_{II}–Ni_I bonds strength decreases less than 1% and the Ni_I–Ni_{Inn} bond strength increases to about 2%. As a consequence of the formed Fe–C interactions, we observed a small Fe–Ni bond weakening while Ni atoms increase its bonding with other neighbouring Ni after C_2H_4 adsorption.

All the orbitals of the ethylene change after adsorption. From Table 2, we can compare the orbital electron occupation for the C_2H_4 molecule before and after adsorption. After adsorption, the C p_x and p_y orbitals undergo depopulation while the C s and p_z populations are increased. The C p_z orbital is the most affected after adsorption, its population increases to about 23% while the rest of the C orbitals are modified less than 8%. The C–Fe interaction involves mainly the overlaps between C p_z orbital and metal s and p orbitals. Fig. 4 shows the major orbital overlap population. This fact is in agreement with the expectation that the p_z orbitals of the carbon are important participant in the frontier molecular orbitals. Also, the C p_z orbitals are more developed than other orbitals. The lobes of these orbitals are well oriented to overlap with the metal s, p_z and $d_z{}^2$ metal orbitals. On the other hand, the 1s orbital population of the hydrogen atoms in the C_2H_4 molecule is affected after adsorption in an amount less than 5%.

Table 3
Major overlap populations for the C_2H_4 adsorption on FeNi(1 1 1) and the changes in the Fe–Fe, Fe–Ni and Ni–Ni bonds.

Bond	OP	Distance (Å)
C_2H_4 on FeNi(1 1 1) according to configuration 1		
C_I–Fe_I	0.123	2.461
C_I–Fe_{II}	0.187	1.735
C_{II}–Fe_{IInn}	0.123	2.461
C_{II}–Fe_{II}	0.182	1.735
Fe_I–Fe_{II}	0.166	2.540
Fe_{II}–Fe_{IInn}	0.155	2.540
Fe_I–Ni_I	0.185	2.540
Fe_{II}–Ni_I	0.160	2.540
Ni_I–Ni_{Inn}	0.277	2.540
C_2H_4 on FeNi(1 1 1) according to configuration 2		
C_I–Fe_I	–	2.579
C_I–Fe_{II}	0.442	1.803
C_{II}–Fe_I	0.437	1.803
C_{II}–Fe_{II}	–	2.579
Fe_I–Fe_{II}	0.100	2.540
Fe_{II}–Fe_{IInn}	0.264	2.540
Fe_I–Ni_I	0.173	2.540
Fe_{II}–Ni_I	0.176	2.540
Ni_I–Ni_{Inn}	0.271	2.540
FeNi(1 1 1) isolated surface		
Fe_I–Fe_{II}	0.262	2.540
Fe_{II}–Fe_{IInn}	0.272	2.540
Fe_I–Ni_I	0.174	2.540
Fe_{II}–Ni_I	0.176	2.540
Ni_I–Ni_{Inn}	0.266	2.540

A detrimental effect on the Fe–Fe bonds is observed after C_2H_4 adsorption on the FeNi(1 1 1) surface. A bond weakening of 37–62% is found for the two major configuration studied. Fig. 5 shows a comparison plot of the Fe–Fe superficial bond, before and after C_2H_4 adsorption. The integration of the Fe–Fe COOP curves up to the Fermi level gives smaller total overlap populations for the chemisorption's systems (Fig. 5(a) and (b)) compared with the clean surface (Fig. 5(c)) confirming the Fe–Fe bond weakening after adsorption.

The possibility of Fe_3C carbide formation was also analyzed. We studied the Fe–C multiple interactions, their corresponding distance and OP values, and no evidence of Fe_3C on the FeNi(1 1 1) surface is observed. In a preliminary work [23] the formation of Fe_3C carbides could be observed in bulk FeNi cluster. A C atom was located near three Fe atoms, at distances of 1.69 Å from two of them and 1.77 Å from the third Fe atom; and the Fe–C OP reported values were 0.752, 0.751 and 0.636 respectively, showing the possibility of Fe_3C carbides formation. The Fe–C average distance in bulk Fe_3C is 2.018 Å [36]. In the case of C_2H_4 on FeNi(1 1 1), the Fe–C distances are longer and the corresponding OP values are smaller (see Table 3) than the Fe–C distances and OPs cited in our previous report confirming that carbide formation is not detected on the FeNi(1 1 1) surface in the early stages of adsorption.

Finally, a comment relevant to the effect of temperature should be mentioned. The theoretical calculations at the atomic scale, starts with an ideal crystal that is studied at zero temperature and low pressure. Pressure is an easy parameter for ab initio (DFT) calculations in contrast to experiments. The opposite is true for estimating temperature effects which is easier for experiment than for theory. Pressure and finite temperature effects can be included using lattice vibrations, which may be approximated from known phonon data. A review that considers the effect of temperature was recently published [37]. In a related paper, the thermally induced decomposition of ethylene to acetyleneon the Ni(1 1 1) surface was treated theoretically: potential-energy curves were computed within a modified extended-Hückel framework and reaction rates estimated via a master equation approach [38].

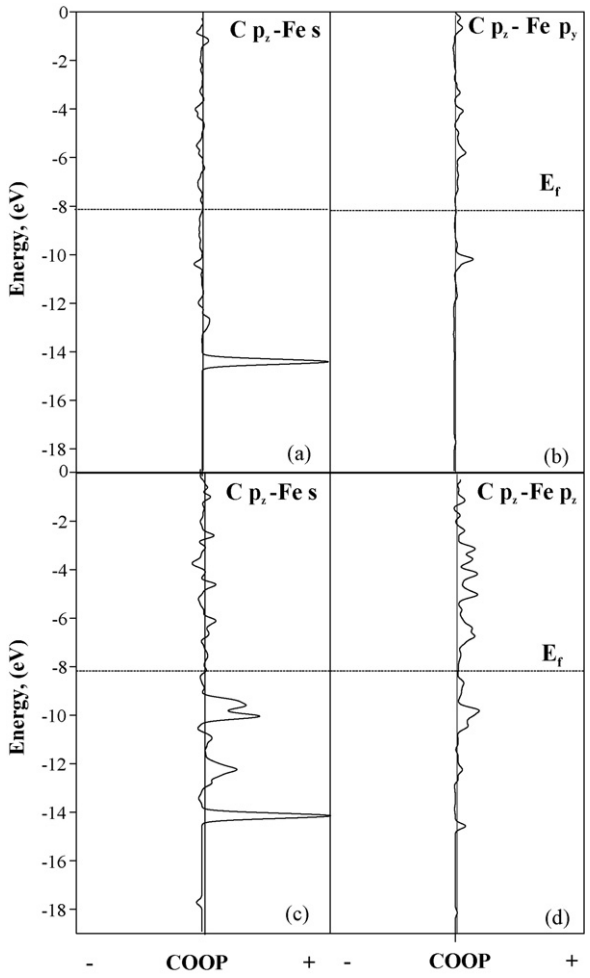

Fig. 4. Major overlap populations between C and Fe orbitals, (a) and (b) for configuration 1, (c) and (d) for configuration 2.

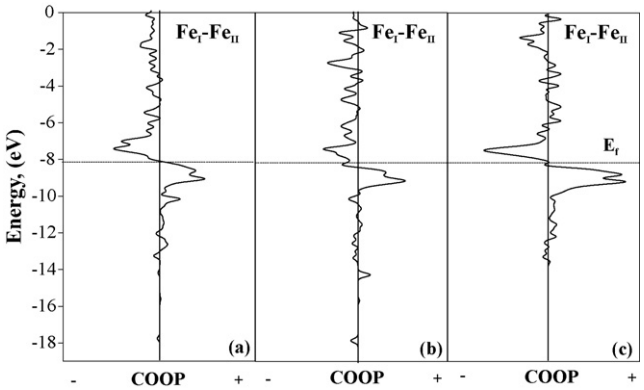

Fig. 5. COOP curves for Fe–Fe interactions (a) configuration 1, (b) configuration 2 and (c) clean FeNi surface.

4. Conclusions

We analyzed at theoretical level, the adsorption of C_2H_4 on FeNi(1 1 1) by tight bonding calculations. Different configurations were selected in order to establish the preferential adsorption site and the optimum molecule-surface distance. The two most stable

sites and geometries for C_2H_4 on FeNi(1 1 1) are those where the C=C bond axis is parallel to the surface along the [1, −1, 0] direction, bonded atop on Fe at 1.60 Å to the surface and the ethylene bonded along the Fe–Fe bridge site at 1.70 Å above the surface.

We found that the minimum energy configuration corresponds to the C=C bonding atop on Fe. C–Fe bonds are formed on the FeNi surface and the interaction is mainly due to the overlaps between the C orbitals with the Fe p_x and p_z orbitals. As a consequence, it is observed a maximum Fe–Fe bond weakening of 43%. On the other hand, the major C–Fe OPs occur when the C atoms are located on the Fe–Fe bridge site. In this case, the C–Fe interactions weaken the Fe–Fe nearest bonds to about 62% with participation of Fe p_y, p_x and p_z orbitals. After adsorption, the Fe–Ni and Ni–Ni bonds are slightly affected. The C–Ni and H's-FeNi(1 1 1) interactions are not relevant and no evidence of Fe_3C carbide like bond on the FeNi(1 1 1) surface is observed.

Acknowledgements

We thank the useful suggestions of the referees. Our work was supported by PIP 0103 (CONICET), PICT 560, 1186 and R656 (ANPCyT), SGCyT-Universidad Nacional del Sur and Universidad Tecnológica Nacional. The authors are members of CONICET-Argentina.

References

[1] O. Altin, S. Eser, Analysis of solid deposits from thermal stressing of a JP-8 fuel on different superalloy surfaces in a flow reactor, Ind. Eng. Chem. Res. 40 (2001) 589–595.
[2] I.M. Allam, Carburization/oxidation behavior of alloy Haynes-214 in methane–hydrogen gas mixtures, Oxid. Met. 72 (2009) 127–144.
[3] C.M. Chun, G. Bhargava, T.A. Ramanarayanan, Metal dusting corrosion of nickel based alloys, J. Electrochem. Soc. 154 (2007) C231–C240.
[4] S. Ando, H. Kimura, Effect of oxide scale on carbon deposition on Fe–Ni alloys in carburizing gas, Metall. Mater. Trans. A 22 (1991) 2393–2399.
[5] C. Park, R.T.K. Baker, Carbon deposition on iron–nickel during interaction with ethylene–carbon monoxide–hydrogen mixtures, J. Catal. 190 (2000) 104–117.
[6] C. Brucker, T. Rhodin, Chemisorption and reaction of acetylene and ethylene on the α-Fe(1 0 0) clean iron surface, J. Catal. 47 (1977) 214–231.
[7] T.N. Rhodin, C. Brucker, A.B. Anderson, Structure and bonding of acetylene and ethylene on alpha-iron surfaces at low temperatures, J. Phys. Chem. 82 (1978) 894–898.
[8] A.B. Anderson, Interaction of hydrogen, carbon, ethylene, acetylene, and alkyl fragments with iron surfaces. Catalytic hydrogenation, dehydrogenation, carbon bond breakage, and hydrogen mobility, J. Am. Chem. Soc. 99 (1977) 696–707.
[9] W.H. Hung, S.L. Bernasek, Adsorption and decomposition of ethylene and acetylene on Fe(1 0 0), Surf. Sci. 339 (1995) 272–290.
[10] W. Erley, A.M. Baro, H. Ibach, Vibrational spectra of acetylene and ethylene adsorbed on Fe(1 1 0), Surf. Sci. 120 (1982) 273–290.
[11] U. Seip, M.-C. Tsai, J. Kuppers, G. Ertl, Interaction of acetylene and ethylene with a Fe(1 1 1), Surf. Sci. 147 (1984) 65–88.
[12] J.M.H. Lo, T. Ziegler, Theoretical studies of the formation and reactivity of C_2 hydrocarbon species on the Fe(1 0 0) surface, J. Phys. Chem. C (2007) 13149–13162.
[13] B. Li, S. Bao, Y. Zhuang, P. Cao, A theoretical study on adsorption geometry of ethylene on the Ni(1 1 0) surface, Phys. B 325 (2003) 92–97.
[14] M. Weinelt, W. Huber, P. Zebisch, H.P. Steinrück, Ethylene adsorbed on Ni(1 1 0): an experimental and theoretical determination of the two-dimensional band structure, Phys. Rev. B 46 (1992) 1675–1686.
[15] X.S. Feng, J.C. Tang, Theoretical investigation of ethylene adsorbed on Ni(1 0 0) surface by the multiple-scattering cluster method, Catal. Let. 20 (1993) 141–148.
[16] R. Neubauer, C.M. Whelan, R. Denecke, H.P. Steinrück, The thermal chemistry of saturated layers of acetylene and ethylene on Ni(1 0 0) studied by in situ synchrotron X-ray photoelectron spectroscopy, J. Chem. Phys. 119 (2003) 1710–1718.
[17] Q. Ge, M. Neurock, Correlation of adsorption energy with surface structure: ethylene adsorption on Pd surfaces, Chem. Phys. Lett. 358 (2002) 377–382.
[18] F. Calaza, F. Gao, Z. Li, W.T. Tysoe, The adsorption of ethylene on Au/Pd(1 1 1) alloy surfaces, Surf. Sci. 601 (2007) 714–722.
[19] H.J. Grabke, Nickel-based alloys in carbonaceous gases, Corrosion 56 (2000) 801–808.
[20] N.M. Rodriguez, M.S. Kim, F. Fortin, I. Mochida, R.T.K. Baker, Carbon deposition on iron-nickel alloy particles, Appl. Catal., A 148 (1997) 265–282.
[21] T. Nakazawa, T. Igarashi, T. Tsuru, Y. Kaji, Ab initio calculations of FeNi clusters, Comput. Mater. Sci. 46 (2009) 367–375.
[22] Y. Mishin, M.J. Mehl, D.A. Papaconstantopoulos, Phase stability in the Fe–Ni system: investigation by first-principles calculations and atomistic simulations, Acta Mater. 53 (2005) 4029–4041.
[23] S. Simonetti, L. Moro, G. Brizuela, A. Juan, A computational study of the carburization phenomena in a Fe–Ni alloy, J. Phys. D: Appl. Phys. 41 (2008) 125006.1–125006.7.
[24] K.B. Reuter, D.B. Williams, J.I. Goldstein, Determination of Fe–Ni phase diagram below 400 °C, Metall. Trans. A 20 (1989) 719–725.
[25] G. Rancourt, R.B. Scorzelli, Low-Spin g-Fe–Ni (gLS) proposed as a new mineral in Fe–Ni-bearing meteorites: epitaxial intergrowth of g_{LS} and tetrataenite as a possible equilibrium state at ≈20–40 at% Ni, J. Magn. Magn. Mater. 150 (1995) 30–36, and references therein.
[26] T. Takahashi, W.A. Bassett, H.K. Mao, Isothermal compression of the alloys of iron up to 300 kbar at room temperature: iron-nickel alloys, J. Geophys. Res. 73 (1968) 4717–4727.
[27] E. Huang, W.A. Bassett, M.S. Weathers, Phase relationships in Fe–Ni alloys at high pressures and temperatures, J. Geophys. Res. 93 (1988) 7741–7746.
[28] H.K. Mao, Y. Wu, L.C. Chen, J.F. Shu, A.P. Jephcoat, Static compression of iron to 300 GPa and $Fe_{0.8}Ni_{0.2}$ alloy to 260 GPa: implication for composition of the core, J. Geophys. Res. 95 (1990) 21737–21742.
[29] J.F. Valderruten, G.A. Peréz Alcázar, J.M. Greneche, Estudio de las aleaciones Fe–Ni producidas por aleamiento mecánico, Rev. Colomb. Fís. 38 (2006) 97–100.
[30] M.-Z. Dang, D.G. Rancourt, Simultaneous magnetic and chemical order-disorder phenomena in Fe_3Ni, FeNi, and $FeNi_3$, Phys. Rev. B 53 (1996) 2291–2302.
[31] A. Anderson, K. Nath, Atom-superposition and electron-delocalization tight-binding band theory, Phys. Rev. B 41 (1990) 5652–5660.
[32] J.F. Valderruten, G.A. Peréz Alcázar, J.M. Greneche, Mossbauer and X-ray study of mechanically alloyed FeNi alloys around the Invar composition, J. Phys. Condens. Matter. 20 (2008) 485204–485210.
[33] W.J. Hehre, L. Radom, P.V.R. Schleyer, J.A. Pople, Ab-initio Molecular Theory, Wiley, New York, 1986.
[34] G. Landrum, W. Glassey, Yet Another extended Hückel Molecular Orbital Package (YAeHMOP), Cornell University, Ithaca, NY, 2004.
[35] V.Z. Mordkovich, E.A. Dolgova, A.R. Karaeva, D.N. Kharitonov, I.A. Maslov, A.A. Kamenev, V.F. Tretjakov, Synthesis of carbon nanotubes by catalytic conversion of methane: competition between active components of catalyst, Carbon 45 (2007) 62–69.
[36] H. Adachi, T. Mukoyama, J. Kawai, Hartree–Fock–Slater Method for Materials Science: The DV-Xa Method for Materials Science, Springer, Germany, 2006.
[37] K. Schwarz, DFT calculations of solids with LAPW and WIEN2k, J. Solid State Chem. 176 (2003) 319–328.
[38] M.E. Lama, R.J. Boyda, H.J. Kreuzer, Mechanism of C_2H_4 dehydrogenation to C_2H_2 on the Ni(1 1 1) surface, Chem. Phys. Lett. 253 (1996) 129–134.